# The Amplitude Phase Decomposition for the Magnetotelluric Impedance Tensor and Galvanic Electric Distortion


Maik Neukirch[1], Daniel Rudolf[2] and Xavier Garcia[1]

[1] Barcelona Center for Subsurface Imaging, Institut de Ciències del Mar, CSIC, Barcelona, Spain
[2] Mathematisches Institut, Universität Jena, Germany



## 1 Abstract

The Phase Tensor marked a breakthrough in understanding and analysis of electric galvanic distortion. It can be used for (distortion free) dimensionality analysis, distortion analysis and subsurface model inversion. However, it does not store impedance amplitude information, therefore the impedance corrected by distortion analysis may yield superior results. We formulate a Magnetotelluric impedance tensor decomposition into Phase and Amplitude Tensor. The new Amplitude Tensor is shown to be complementary and independent of the Phase Tensor and to contain galvanic and inductive information, which the latter is physically related to the Phase Tensor. This physical similarity is used to approximate the galvanic amplitude for a general subsurface, leading to: (i) the galvanic response may have a changing impact on the impedance over a period range and (ii) only the galvanic response of the lowest period should be termed galvanic distortion. The galvanic amplitude approximation offers a new perspective on galvanic distortion, which breaks with the general belief of the need to assume 1D/2D regional structure. The Amplitude Tensor is illustrated and compared to the Phase Tensor on real and synthetic examples.


## 2 Introduction and Motivation

Galvanic electric distortion is a long standing problem for the magnetotelluric (MT) method [Berdichevsky and Dmitriev, 1976, Jiracek, 1990, Jones, 2011]. Two main remedies have emerged: (i) modelling near surface inhomogeneities or their effects, and accounting for them [Miensopust, 2010, Avdeeva et al., 2015], and (ii) analytic solutions based on structural assumptions (2D) on the impedance tensor [Groom and Bailey, 1989, McNeice and Jones, 2001, Jones, 2012]. Modelling of distortion effect has grown popular since Caldwell et al. [2004] introduced the distortion free Phase Tensor and Bibby et al. [2005] showed that previous solutions on distortion analysis contain implicit assumptions on the distortion matrix and not only the explicit structural impedance constraint (be it 1D or 2D) concluding that distortion analysis cannot be uniquely resolved without assumptions on the distortion matrix itself.

Given the Phase Tensor [Caldwell et al., 2004], we propose a complementary Amplitude Tensor to represent the impedance. Both tensors are independent and exhibit significant structural similarity corresponding to the present subsurface, even if 3D. Amplitude Tensor properties are described and its similarity to the Phase Tensor is demonstrated in terms of regional subsurface strike angle, dimensionality and anisotropy. Since the Amplitude Tensor combines galvanic distortion and regional amplitude, we postulate that the latter can be approximated by Phase Tensor properties, allowing to estimate distortion up to a constant without regional dimensionality assumptions or explicit constraints on the distortion matrix.

## 3 Amplitude Phase Decomposition

Let $Z \in \mathbb{C}^{n\times n}$ be represented in analogy to the polar form of complex numbers $z = \varrho \cdot \exp(i\varphi)$with matrices ($P$, $\mathbf{\Phi}$, $C$, $S$ and $E$) analogue to $\varrho$, $\varphi$, $\cos\varphi$, $\sin\varphi$ and $\exp(i\varphi)$:

$$Z = PE = P(C + iS). \tag{1}$$

In particular, the sum of squares of the amplitude independent terms shall be unity in analogy to the trigonometric identity:

$$C \cdot C^T + S \cdot S^T = I. \tag{2}$$

Then, (1), (2), $Z = X + iY$ and $\mathbf{\Phi} = X^{-1}Y$ yield

$$C = \left(\mathbb{I} + \mathbf{\Phi\Phi}^T\right)^{-\frac{1}{2}}, S = \left(\mathbb{I} + \mathbf{\Phi\Phi}^T\right)^{-\frac{1}{2}} \cdot \mathbf{\Phi}, E = C + iS.$$

Hence, a unique, real-valued Amplitude Tensor can be defined as

$$P = Z \cdot E^{-1}. \tag{3}$$

Then, we follow the matrix parameterization by Booker [2014]:

$$M = R(-\theta_M) \cdot \mathrm{diag}(m_1, m_2) \cdot R(\psi_M) \cdot R(\theta_M) \tag{4}$$

for the strike $\theta_M$, the singular values $m_{1/2}$ and the skew $\psi_M$.

## 4 Example of Tensor Parameter

As an example, we chose site *A09* of the Dublin Secret Model One [DSM1, Miensopust et al., 2013], because the data are: (i) noise-free, (ii) distortion-free and (iii) truly 3D with two differently oriented 2D structures at different depths. Visual inspection of the impedance data (panels 1a and 1b) shows equal off-diagonal amplitude and very small diagonal elements for the first three periods. After the fourth period off-diagonal elements differ and main diagonal elements begin to be significant after the sixth period (around **10** s), translating into the observation that the data is roughly 1D for the first three periods, roughly 2D till the sixth and increasingly 3D thereafter. Examination of the phase tensor skew (panel 1c) the data is seen as 3D after the eighth period (considering a maximum skew of $\pm\mathbf{6}°$ as suggested by Booker [2014]) and return to lower dimensionality (presumably 2D) at the twelfth period ($\approx$ **500** s). However, further examination of the Phase Tensor strike angle (panel 1d) reveals that any apparent two-dimensionality would change orientation and thus, 2D should not be assumed if the near surface 2D data and deep 2D data are to be interpreted (inverted) jointly. Therefore, the given example ranges from 1D to 3D, including an orientation change of a 2D structure which in fact is the cause of the 3D effect.

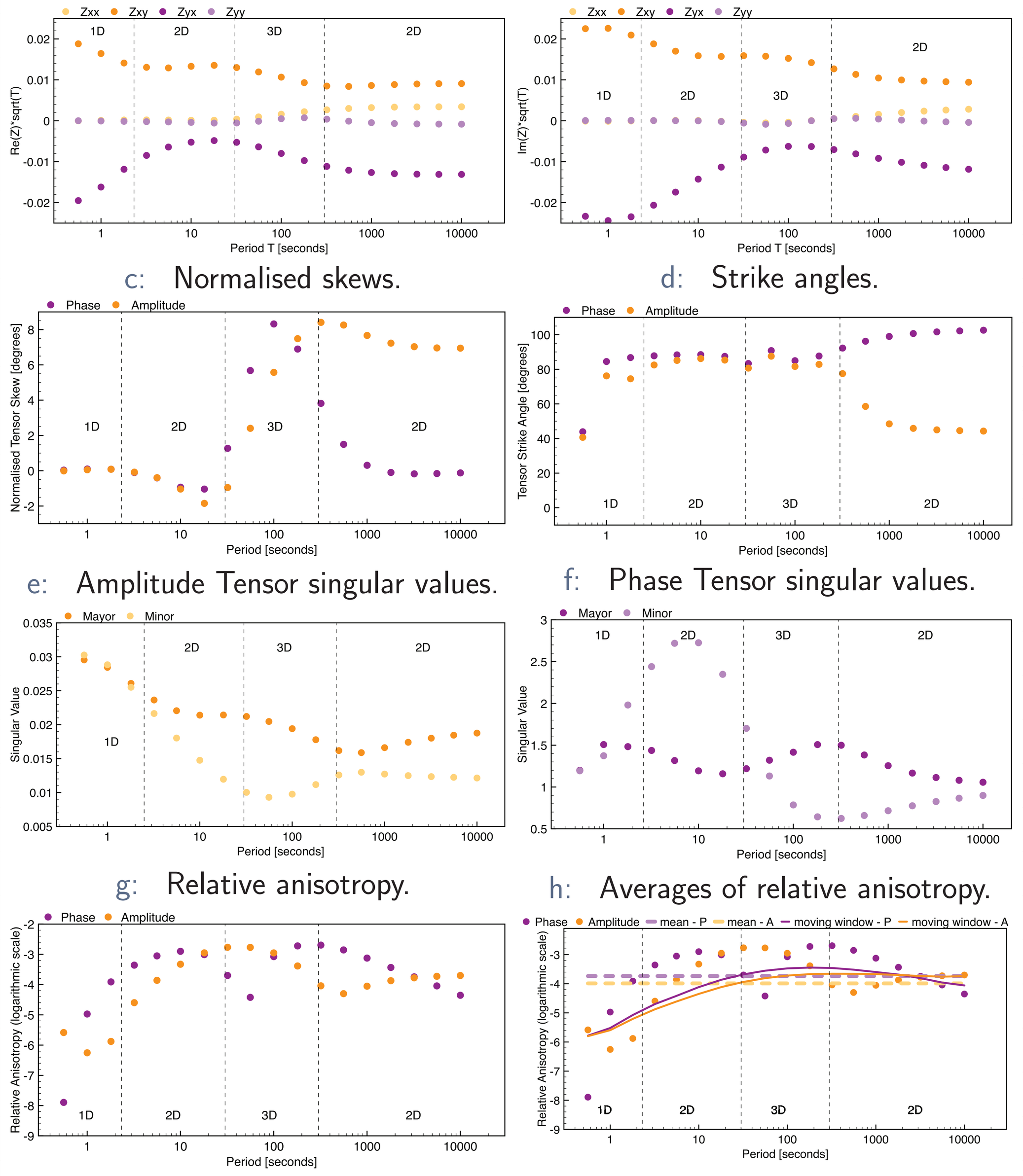


Figure 1: Impedance data of site *A09* of the DSM1 [Miensopust et al., 2013] is decomposed in Phase and Amplitude Tensor skew, strike and singular values. Note that the amplitude skew is normalised in order to account for diagonal versus off-diagonal nature of phase and Amplitude Tensor ($\phi_P^{\mathrm{norm}} = 90° - \phi_P$).

## 5 Relative Logarithmic Anisotropy

Consider the following two anisotropy definitions:

$$\phi_a = \frac{1}{2}(\tan^{-1}(\phi_1) - \tan^{-1}(\phi_2)), \tag{5}$$

$$\rho_a = \frac{1}{2}(\ln(\rho_1) - \ln(\rho_2)). \tag{6}$$

In order to compare Amplitude and Phase, it is imperative that the scales of both are comparable (cp. Figure 1g and h). Since the real and imaginary parts of the logarithm of complex numbers $z = \rho\exp(i\phi)$ relate to the logarithm of the amplitude $\rho$ and phase $\phi$ respectively, we argue that these measures are as comparable as real and imaginary parts of the logarithm of complex numbers:

$$\ln z = \ln(\rho\exp(i\phi)) = \ln\rho + i\phi. \tag{7}$$

## 6 Dublin 3D Modelling and Inversion Workshop Synthetic Models

The Secret Model 1 (2008) in Figure 2a features a **100** $\Omega$m background with a (**1** $\Omega$m) body starting at North-East, then spiraling down towards, at first West, then South, East and finally North (to the left). At highest periods, only the phase senses the shallowest part in North-East. At (**32** s), the lag between amplitude and phase becomes clear and the phase begins to lose sensitivity towards smaller scales. Phase dimensionality peak (skew angle) is reached at around **560** s revealing the complexity of the model. When phase sensitivity has diminished, the amplitude reluctantly adapts to deeper structure and continues to recognise dominant shallow structure of the integrated model and therewith illustrating the present galvanic effect in the amplitude.

Figure 2b displays a selection of periods from a complex, large scale model that will be discussed at the workshop in June 2016 and specifics are not yet public. The model represents a ocean-continent setting inspired by the US West coast, includes bathymetry and topography and is noted as showing strong ocean effects. At **40** s, amplitude and phase note severe coastal effects and numerous shallow anomalies but at **40000** s, almost all phase information is aligned with the coastline, whereas the (galvanic) amplitude shows the dominant features of the model.

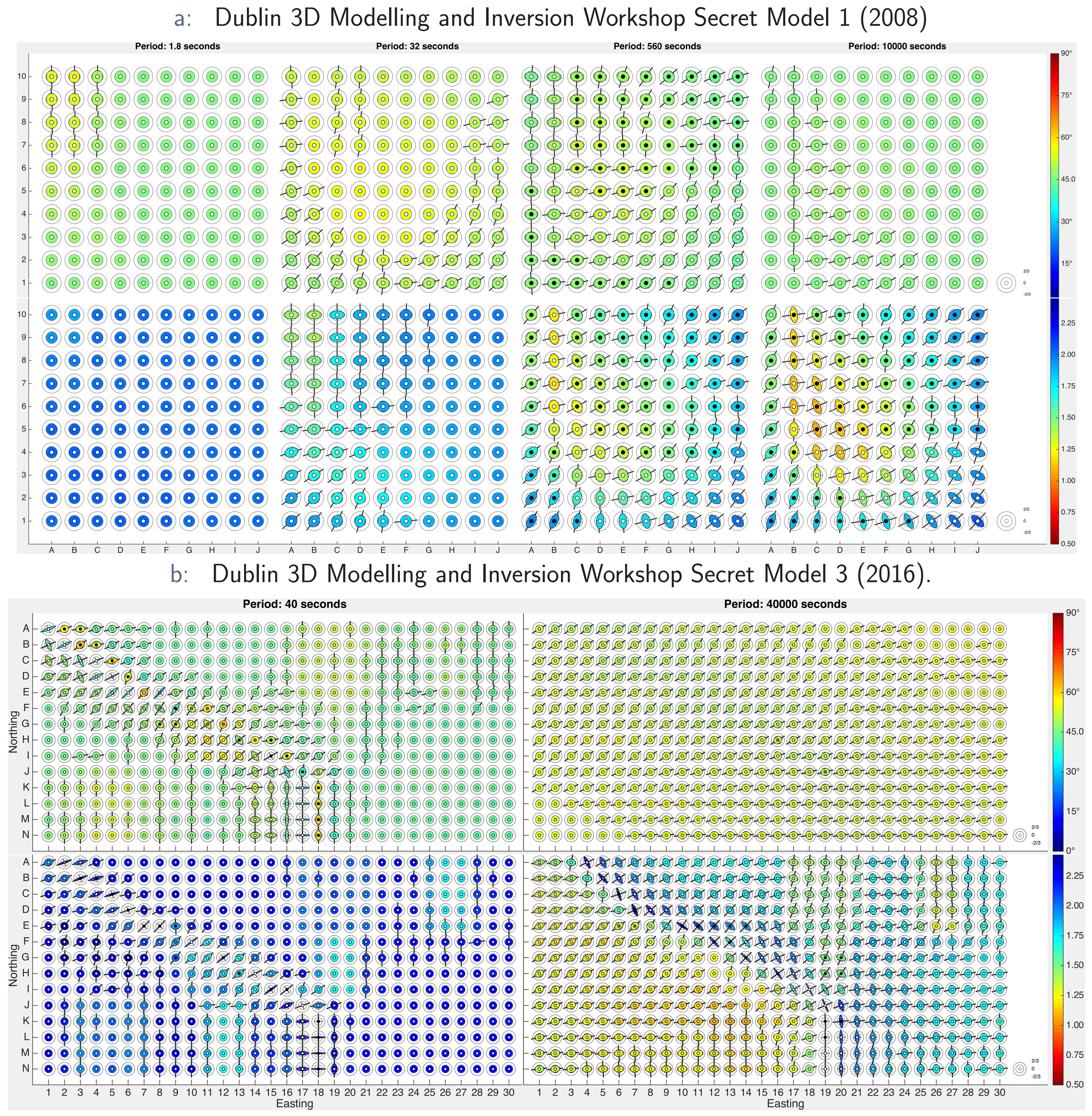


Figure 2: Phase (upper) and Amplitude (lower) Tensor are illustrated by determinant (degrees and log. apparent resistivity in color), qualitative skew (circle fill - black/grey/white (3D/quasi 2D/2D)), anisotropy and strike (ellipse).

## 7 Estimating Inductive and Galvanic Amplitude From the Phase Tensor

Consider a 2D impedance tensor in regional strike coordinates, with the two principal components:

$$Z_{1/2} = \exp(\ln\rho_{1/2} \pm i\tan^{-1}\phi_{1/2}) \tag{8}$$

with the singular values $\rho_1$, $\rho_2$ and $\phi_1$, $\phi_2$ of Amplitude and Phase Tensor, respectively. Let

$$\rho = \exp\left(\frac{1}{2}(\ln\rho_1 + \ln\rho_2)\right) \tag{9}$$

$$\phi = \left(\frac{1}{2}(\tan^{-1}\phi_1 + \tan^{-1}\phi_2)\right), \tag{10}$$

then we obtain:

$$Z_{1/2} = \exp(\ln\rho \pm \rho_a) \pm i(\phi \pm \phi_a)))$$

where $\phi_a$ and $\rho_a$ are the phase and logarithmic amplitude anisotropy. For real data, both, $\phi$ and $\phi_a$ are generally unaffected by electric field distortion, whereas $\rho$ can include galvanic shift (constant multiplicative factor) and $\rho_a$ may include galvanic anisotropy. Assuming that the inductive response of the subsurface has a similar effect on Phase and Amplitude, we can estimate the inductive amplitude singular values by

$$\rho_{1/2}^{\mathrm{ind}} = \exp(\ln\rho \mp \phi_a) \tag{11}$$

and the galvanic amplitude singular values by

$$\rho_1^{\mathrm{gal}} = \exp(\pm(\rho_a + \phi_a)) \tag{12}$$

In a general 3D situation, we can follow the same logic and additionally assume similar geologic strike (and subsurface dimensionality) for inductive amplitude and phase. Therewith, by substituting phase strike (skew) as inductive amplitude strike (skew) and the singular values as in the 2D example, we obtain an estimate for the galvanic Amplitude Tensor which represents purely galvanic subsurface information:

$$P^{\mathrm{gal}} = P \cdot \left(P^{\mathrm{ind}}\right)^{-1}. \tag{13}$$

## 8 Real Data Example: SAMTEX

Here we present how Amplitude Tensor properties could be used to obtain qualitative real data interpretations. Figure 3 shows a parameter map of the SAMTEX dataset [Evans et al., 2011]. Logarithmic apparent resistivities (colored ellipses) correspond to Kaapvaal and Zimbabwe Archaean terranes and Ghanzi-Chobe belt with higher values (cooler colors), and lower values (warmer colors) for some of the Phanerozoic terranes, like the Rehoboth terrane, already pointed out by Evans et al. [2011]. In particular the northern Rehoboth terrane border and the data collected in Namibia, on the Damara and Ghanzi-Chobe belts, are marked by high resistivities, which correlate with 2D inversion results from Muller et al. [2009].

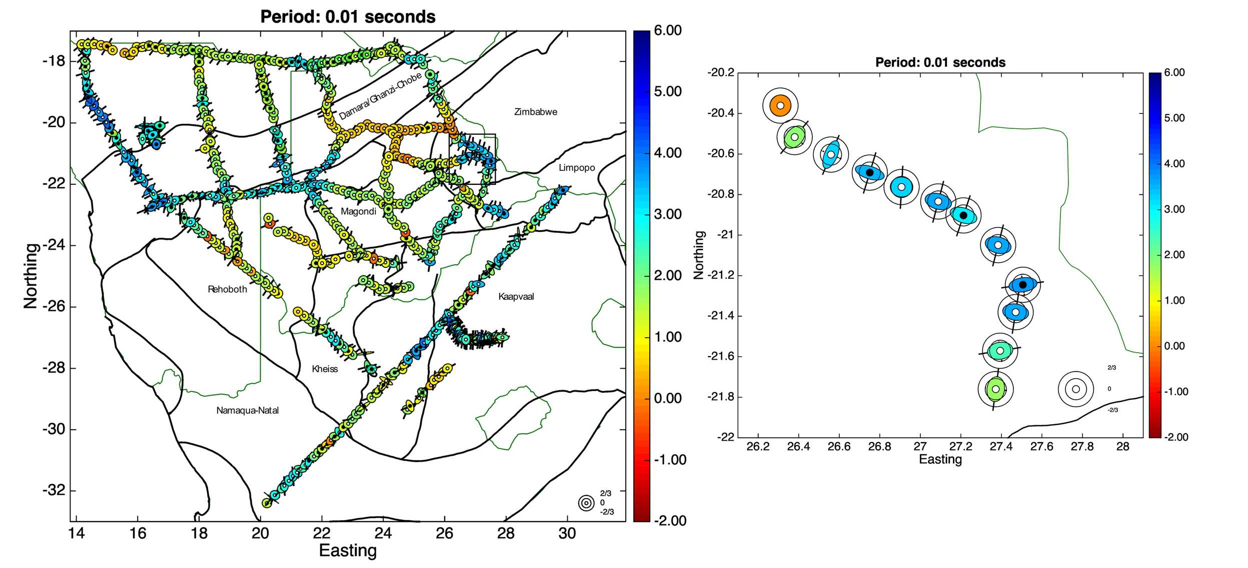


Figure 3: Amplitude Tensor map of the SAMTEX experiment illustrated by determinant (logarithmic apparent resistivity in color), skew, anisotropy and strike angle (as above). On the right, there is a zoom of a few sites located in the area under the rectangle on the left plot.

## 9 Conclusion

We newly define an Amplitude Tensor and demonstrate its properties and complementarity to the Phase Tensor (i.e. for modeling or mapping). The physical relation between Phase and inductive Amplitude Tensor leads to a galvanic amplitude approximation with the following qualitative interpretation of general 3D distortion: (i) the galvanic response may have a changing impact on the impedance over a period range and (ii) only the galvanic response of the lowest period should be termed galvanic distortion.


## Acknowledgement

This work was funded by Repsol under the framework of the CO-DOS project. All MT3D workshop datasets are publicly available at `http://mtnet.dias.ie/workshops/em_workshops.html` with further details. For this we especially thank the workshop organisers and the model creators, Alan Jones, Marion Miensopust, Pilar Queralt and Jan Vozar.


## References


M N Berdichevsky and V I Dmitriev. Distortion of magnetic and electric fields by near-surface lateral inhomogeneities. *Acta Geod. Geophys. Montan. Acad. Sci. Hung*, 11:447–483, 1976.

G R Jiracek. Near-surface and topographic distortions in electromagnetic induction. *Surveys in Geophysics*, 11(2-3): 163–203, 1990.

A G Jones. Three-dimensional galvanic distortion of three-dimensional regional conductivity structures: Comment on "Three-dimensional joint inversion for magnetotelluric resistivity and static shift distributions in complex media" by Y Sasaki and M A Meju. *Journal of Geophysical Research*, pages 1–5, 2011.

M P Miensopust. Multidimensional magnetotellurics: A 2d case study and a 3d approach to simultaneously invert for resistivity structure and distortion parameters. *PhD thesis*, 2010.

A Avdeeva, M Moorkamp, D Avdeev, M Jegen, and M Miensopust. Three-dimensional inversion of magnetotelluric impedance tensor data and full distortion matrix. *Geophysical Journal International*, 202(1):464–481, 2015. doi: 10.1093/gji/ggv144.

R W Groom and R C Bailey. Decomposition of Magnetotelluric Impedance Tensors in the Presence of Local Three-Dimensional Galvanic Distortion. *Journal of Geophysical Research*, 94(B2):1913–1925, 1989.

G W McNeice and A G Jones. Multisite, multifrequency tensor decomposition of magnetotelluric data. *Geophysics*, 66 (1):158–173, 2001.

A G Jones. Distortion decomposition of the magnetotelluric impedance tensors from a one-dimensional anisotropic earth. *Geophysical Journal International*, 189(1):268–284, 2012.

T G Caldwell, H M Bibby, and C Brown. The magnetotelluric phase tensor. *Geophysical Journal International*, 158(2): 457–469, 2004. doi: 10.1111/j.1365-246X.2004.02281.x.

H M Bibby, T G Caldwell, and C Brown. Determinable and non-ï¿½ï¿½determinable parameters of galvanic distortion in magnetotellurics. *Geophysical Journal International*, 163(3):915–930, 2005.

J R Booker. The magnetotelluric phase tensor: A critical review. *Surveys in Geophysics*, 35(1):7–40, 2014. doi: 10.1007/s10712-013-9234-2.

M P Miensopust, P Queralt, A G Jones, and the 3D MT modellers. Magnetotelluric 3-d inversion: a review of two successful workshops on forward and inversion code testing and comparison. *Geophysical Journal International*, 193(3): 1216–1238, 2013. doi: 10.1093/gji/ggt066.

R L Evans, A G Jones, X Garcia, M Muller, M Hamilton, S Evans, CJS Fourie, J Spratt, S Webb, H Jelsma, and the SAMTEX TEAM. Electrical lithosphere beneath the Kaapvaal craton, southern Africa. *Journal of Geophysical Research: Solid Earth*, 116(B4):1978–2012, 2011.

Mark R. Muller, Alan G. Jones, Robert L. Evans, Herman S. Grütter, Chris Hatton, Xavier Garcia, Mark P. Hamilton, Marion P. Miensopust, Patrick Cole, Tiyapo Ngwisanyi, Dave Hutchins, C. J. Stoffel Fourie, Hielke A. Jelsma, Shane F. Evans, Theo Aravanis, Wayne Pettit, Susan J. Webb, and Jan Wasborg. Lithospheric structure, evolution and diamond prospectivity of the Rehoboth Terrane and western Kaapvaal Craton, southern Africa: Constraints from broadband magnetotellurics. *Lithos*, 112:93–105, 2009. doi: 10.1016/j.lithos.2009.06.023.